# Proton NMR Assignments and Solution Conformation of RANTES, a Chemokine of the C-C Type†

Nicholas J. Skelton,*,‡ Fernando Aspiras,§ John Ogez,§ and Thomas J. Schall||,⊥

*Departments of Protein Engineering, Process Sciences, and Immunology, Genentech, Inc., South San Francisco, California 94080*

*Received October 31, 1994; Revised Manuscript Received February 16, 1995*®

ABSTRACT: $^1$H NMR has been used to investigate the structural properties of RANTES, a protein from the C-C branch of the chemotactic cytokine family that has a strong chemoattractive effect on monocytes, lymphocytes, and eosinophils. Titration of pH from 5.0 to 2.5 indicates that RANTES is extensively aggregated in solution above pH 4.0. At pH 3.7 the protein is mostly dimeric, although this species does dissociate to the monomer with a $K_d$ of 35 $\mu$M. NMR data have been acquired and resonance assignments made for the dimeric species. Structures of the dimer have been generated by distance geometry and simulated annealing calculations that utilized 1956 intramolecular distance restraints, 120 intermolecular distance restraints, 164 dihedral angle restraints, and 68 restraints enforcing 34 hydrogen bonds (17.0 restraints per residue). The structure is well-defined (average root mean square deviation from the average structure of 0.38 ± 0.06 and 0.53 ± 0.12 Å for backbone heavy atoms of residues 4−66 of the monomer and dimer, respectively). Each monomer consists of a C-terminal α-helix packing against a three-stranded antiparallel β-sheet and two short N-terminal β-strands; dimerization occurs between the N-terminal regions of each monomer. This quaternary structure is very different from that of the C-X-C chemokines such as interleukin-8 and melanoma growth stimulatory activity but similar to that found for the C-C chemokine macrophage inflammatory factor 1β. Distinct structural differences between RANTES and other chemokines at both the tertiary and quaternary level are discussed with regard to the distinct biological functions of the C-C and C-X-C members of this protein family.

The chemokines are a family of small proteins (ca. 70 residues) produced by a variety of mammalian cells that are able to induce chemotaxis and activation of leukocytes (Lindley et al., 1993; Schall, 1994). All of the members of this family have a number of conserved cysteine residues, and they can be partitioned into subfamilies on the basis of primary sequence: proteins in the "C-X-C" branch contain one residue between the two cysteines nearest to the N-terminus, proteins in the "C-C" branch contain adjacent cysteine residues near the N-terminus, and proteins in the "C" branch lack the first and third of the four cysteine residues conserved in the other branches (Kelner et al., 1994). Proteins such as IL-8,[1] MGSA (GRO-α), GRO-β, PF-4, IP-10, and NAP-2 belong to the C-X-C branch and are able to act as chemoattractants for neutrophils but not monocytes or lymphocytes. The proteins RANTES, MCP-1, MCP-2, MIP-1α (LD-78), and MIP-1β (Act-2) are members of the C-C branch and are variously responsible for chemotaxis of monocytes, lymphocytes, and eosinophils but not neutrophils. Some proteins from both subfamilies are also able to attract basophils and eosinophils, although the activity of the C-C proteins is often more pronounced. Lymphotaxin is the first example of a protein from the C branch, and it shows chemotactic activity toward lymphocytes (Kelner et al., 1994). In addition to chemotactic activity, the chemokines are able to promote a number of other biological functions of leukocytes such as intracellular calcium release, respiratory burst, exocytosis, and cell adhesion. The cellular production of these proteins and their particular biological effects have been extensively reviewed (Oppenheim et al., 1991; Schall, 1991, 1994; Miller & Krangel, 1992; Baggiolini et al., 1994).

Because of the ability to attract and activate leukocytes, members of the chemokine family are thought to play an important role in initiating or maintaining inflammatory responses (Butcher, 1991; Schall, 1994; Springer, 1994). Such a response in joint, skin, or lung tissue often has serious clinical implications. Thus, the last several years have seen much research aimed at understanding the complex interplay between these proteins and their various receptors [e.g., see Hébert et al. (1991, 1993), Lee et al. (1992), Moser et al. (1993), Neote et al. (1993a,b), and Clark-Lewis et al. (1994)].

† Coordinates have been deposited in the Brookhaven Protein Data Bank under accession codes 1RTN for the ensemble and 1RTO for the minimized mean structure.

* To whom correspondence should be addressed.
‡ Department of Protein Engineering.
§ Department of Process Sciences.
|| Department of Immunology.
⊥ Present address: DNAX Research Institute of Molecular and Cellular Biology, 901 California Ave., Palo Alto, CA 94304.

® Abstract published in *Advance ACS Abstracts,* April 1, 1995.

[1] Abbreviations: 2(3)Q, two- (three-) quantum spectroscopy; COSY, correlation spectroscopy; COSY-35, COSY spectrum acquired with a 35° detection pulse; DG, distance geometry; FID, free induction decay; HIC, hydrophobic interaction chromatography; IL-8, interleukin-8; JR-NOESY, NOESY spectrum acquired with the final 90° pulse replaced by a jump and return sequence; MCP, monocyte chemoattractant protein; MGSA, melanoma growth stimulatory activity; MIP, macrophage inflammatory protein; NCS, noncrystallographic symmetry; NMR, nuclear magnetic resonance; NOE, nuclear Overhauser effect; PF4, platelet factor 4; RANTES, *r*egulated upon *a*ctivation, *n*ormal *T*-cell *e*xpressed and presumably *s*ecreted; rEM, restrained energy minimization; RMSD, root mean square deviation; ROESY, rotating frame Overhauser effect spectroscopy; SA, simulated annealing; TOCSY, total correlation spectroscopy; TPPI, time-proportional phase incrementation.

0006-2960/95/0434-5329$09.00/0 

In order to rationalize the wealth of functional data, structural studies have been undertaken by both NMR and X-ray crystallography. The crystal structure of bovine PF4 was solved and found to contain a tetrameric arrangement of polypeptide chains (St. Charles et al., 1989). In solution, IL-8 was found to be dimeric (containing half of the intermolecular interactions observed for PF4) and consisted of a six-stranded antiparallel $\beta$-sheet with two helices packed across the sheet; three strands and one helix are contributed from each monomer (Clore et al., 1989). This structure provided a starting point for modeling studies of other chemokines and speculation of the functionally important areas of the structure (Gronenborn & Clore, 1991). More recently, structures have also been reported for human PF-4 (Zhang et al., 1994), MGSA (Fairbrother et al., 1994; Kim et al., 1994), and MIP-1$\beta$ (Lodi et al., 1994); in all cases, the monomeric motif is similar to that of IL-8 (a C-terminal helix atop three antiparallel $\beta$-strands), although the quaternary contacts have been found to vary.

In order to extend the structural database of chemokines, we have used NMR to study RANTES, a member of the C-C chemokine subfamily. This protein is produced primarily in lymphocytes (Schall et al., 1988), and in addition to chemoattraction of monocytes (Schall et al., 1990), it is also a potent attractant for lymphocytes (Schall et al., 1990), basophils, and eosinophils (Kameyoushi et al., 1992; Rot et al., 1992). Speculation has surrounded the involvement of RANTES in respiratory pathologies, and recently a causative role of RANTES in the generation of eosinophil nasal polyps has been suggested (Beck et al., 1994). These unusual properties make RANTES an interesting target for structure–function analysis, and the structure reported herein provides a starting point for such investigations. In addition, comparison of the RANTES structure with the structure of other chemokines allows a prediction of the molecular elements of these proteins required for receptor interaction.

## MATERIALS AND METHODS

*Sample Preparation.* RANTES was overexpressed in *Escherichia coli* as previously described (Kuna et al., 1992). Cell paste (1200 g) was dispersed in 5 volumes of 50 mM glycine and 250 mM NaCl buffer (pH 3). Following cell disruption, the material was centrifuged for 30 min at 4500 rpm. After the pH was adjusted to 6.0, the supernatant was recentrifuged, filtered, and loaded onto a cation-exchange column (S-Sepharose Fast Flow, Pharmacia) equilibrated with sodium citrate buffer (20 mM, pH 6.0) and eluted with a 0–1 M NaCl gradient. Protein-containing fractions were pooled and loaded onto an HIC column (Phenyl ToyoPearl, 650 $\mu$m, Tosohaas) equilibrated with ammonium sulfate (1.8 M) and sodium phosphate (100 mM, pH 6) and eluted with a linear gradient to 1.5 M ammonium sulfate. The HIC pool was acidified to pH 3 with phosphoric acid and further purified by preparative HPLC (Vydac C18 column) using a gradient of 23–35% acetonitrile in 50 mM acetic acid and 100 mM NaCl buffer. Pure protein was obtained after a final cation-exchange step (S-Sepharose Fast Flow column) equilibrated with 50 mM acetic acid and 50 mM NaCl and eluted with sodium citrate (200 mM, pH 6) and a NaCl gradient. Salts were removed by dialyzing twice against 50 mM acetic acid. The protein was judged pure by analytical HPLC (0.1% trifluoroacetic acid, acetonitrile gradient) and had the expected molecular weight by mass spectrometry (calculated $M + H^+ = 7846.9$, observed = 7847.0).

Storage of the protein above pH 4.5 resulted in gradual precipitation. The precipitate could be reconstituted by dissolving in 6 M guanidine hydrochloride followed by dialysis against 25 mM acetate buffer at pH 4.0. Protic buffer was replaced with deuterated acetate by repeated dilution with acetate-$d_3$ and concentration in a Centriprep-10 (Amicon). Final samples used for NMR experiments in $H_2O$ solution contained 3.0–4.0 mM protein in 25 mM deuterated acetate, 5% (v/v) $D_2O$, and 0.1 mM $NaN_3$ at pH 3.7. $H_2O$ was exchanged for $D_2O$ by elution through a PD-10 gel filtration column (Pharmacia) preequilibrated with 25 mM acetate-$d_3$ in $D_2O$ at pH 3.7 (uncorrected) containing 0.1 mM $NaN_3$. Fractions containing protein were pooled and concentrated in Centricon-10 (Amicon) at 5 °C to yield a final protein concentration of 4.0 mM. Concentrations were determined by UV absorption at 276 nm, using a molar extinction coefficient of 10 850 absorbance units·$cm^{-1}$.

*Dynamic Light Scattering.* Data were collected on a DynaPro-801 (Protein Solutions Inc., High Wycombe, U.K.) instrument at 25 °C. Samples were prepared at a variety of concentrations and pH values in 25 mM acetate-$d_3$ buffer. The data were initially fit assuming a unimodal distribution of molecular size. Samples determined to be polydisperse were usually better fit by a bimodal distribution of molecular sizes. Data fitting and conversion of hydrodynamic radii to molecular weights were performed by the DynaPro-801 software version 4.0, as described in the operator's manual.

*NMR Spectroscopy.* All spectra were acquired at 308 K on a Bruker AMX-500 spectrometer. COSY (Aue et al., 1975), 2Q (Braunschweiler et al., 1983; Rance & Wright, 1986), NOESY (Kumar et al., 1980; Bodenhausen et al., 1984), ROESY (Bothner-By et al., 1984), and TOCSY (Braunschweiler & Ernst, 1983; Bax & Davis, 1985) spectra were acquired from $H_2O$ and $D_2O$ solution. In addition, a JR-NOESY (Plateau & Guéron, 1982) spectrum was acquired from $H_2O$ solution, and COSY-35 (Bax & Freeman, 1981), 2QF-COSY (Rance et al., 1983), and 3Q (Braunschweiler et al., 1983) spectra were acquired from $D_2O$ solution. All data were complex in $\omega_2$, and phase discrimination in $\omega_1$ was achieved with TPPI (Marion & Wüthrich, 1983). In all spectra (except the JR-NOESY), water suppression was achieved by coherent low-power irradiation of the water resonance prior to the pulse sequence for 1.5–2.0 s and during the NOESY mixing time of data acquired from $H_2O$ solution. NOESY, JR-NOESY, and TOCSY spectra were acquired as described previously (Akke et al., 1991); in addition, first-order phase corrections were avoided by acquisition in a sine-modulated fashion in $\omega_1$. TOCSY mixing was achieved with a clean DIPSI-2rc sequence applied for 14, 35, or 75 ms (Cavanagh & Rance, 1992). NOESY spectra were collected with mixing times of 50 and 100 ms (200 ms for the JR-NOESY). ROESY spectra were collected with a spin-lock field strength of 4 kHz applied for 35 ms.

Slow amide proton exchange with solvent was measured by repeated acquisition of TOCSY spectra in a sample freshly prepared in $D_2O$ (see above). After the protein first came into contact with $D_2O$, 70 min elapsed before acquisition of the first TOCSY spectrum. This time was composed of 5 min at 20 °C (gel filtration), 50 min at 5 °C (concentration), and 15 min at 35 °C (spectrometer tuning and calibration).

Each TOCSY required a total acquisition time of 12 min (four scans for each of 128 $t_1$ increments).

*Data Processing and Analysis.* The spectra were processed and analyzed using Felix (Biosym Technology, San Diego, CA). Prior to Fourier transformation in $t_2$, each FID was corrected for DC offset using the final 5% of the FID, the first point was linear predicted and halved in intensity (Otting et al., 1986), and the FID was multiplied by a weak Lorentzian-to-Gaussian window function. In $t_1$, the first point of cosine-modulated data was multiplied by 0.5 and the interferogram multiplied by a cosine bell followed by the application of a weak Lorentzian-to-Gaussian function; the interferograms were zero-filled to yield 1024 real points in each column of the matrix.

*Distance and Dihedral Angle Restraints.* Cross-peaks in the ROESY spectra ($H_2O$ and $D_2O$) were categorized as strong, medium, or weak on the basis of the integrated volume and assigned upper bounds of 2.7, 3.3, or 4.2 Å, respectively. Cross-peaks not present in the ROESY spectra that were observed in the NOESY experiments ($\tau_m = 50$ ms in $D_2O$ and $\tau_m = 100$ ms in $H_2O$) were categorized in a similar fashion and assigned upper bounds of 3.3, 4.2, or 5.5 Å. Cross-peaks in the $H_2O$ NOESY within 0.2 ppm of the water resonance in $\omega_1$ were assigned an upper bound on the basis of the intensity in the JR-NOESY spectrum. In all spectra, the restraint distance used for overlapped cross-peaks was increased by one category or set to the maximum upper bound, depending on the severity of the overlap. Cross-peak volumes involving methyl groups, degenerate methylene resonances, and protons of rapidly flipping aromatic side chains were divided by the number of protons contributing to the resonance before categorization (Yip, 1990).

$^3J_{HN-H\alpha}$ scalar coupling constants were determined from high digital resolution COSY spectra, with $\omega_2$ cross sections through $H^N-H^\alpha$ correlations analyzed by a nonlinear least-squares fitting routine (Neil Jacobsen and Joshua Theaker, unpublished results). $\phi$ backbone dihedral angles were restrained to $-90°$ to $-40°$ if $^3J_{HN-H\alpha}$ was less than 6.0 Hz and $-150°$ to $-90°$ if $^3J_{HN-H\alpha}$ was greater than 8.0 Hz. For non-glycine residues in which $^3J_{HN-H\alpha}$ could not be measured or was in the range 6.0−8.0 Hz, $\phi$ was restrained to be negative if the intraresidue $H^N-H^\alpha$ NOE was less intense than the sequential $H^\alpha-H^N$ NOE (Clubb et al., 1994).

Side chains in which $H^\alpha-H^{\beta1}/H^\alpha-H^{\beta2}$ cross-peak intensity ratios were greater than 5 in short mixing time (14 ms) $D_2O$ TOCSY experiments were assumed to have fixed $\chi_1$ rotamer positions with one large and one small $^3J_{H\alpha-H\beta}$; the $\chi_1$ angle of such side chains was restrained to be between 120° and 360°. Estimation of $^3J_{H\alpha-H\beta}$ in this way is analogous to the method described by Clore et al. (1991). Side chains in which both $H^\alpha-H^\beta$ cross-peaks were weak had $\chi_1$ restrained between 0° and 120°. The direct measurement of $^3J_{H\alpha-H\beta}$ in the COSY-35 spectrum for 12 side chains permitted calibration of this scheme; however, low signal-to-noise ratios (presumably because of cancellation of antiphase cross-peak components) precluded direct measurement for the majority of side chains. Stereospecific assignments of groups were made by manual observation of intraresidue and sequential ROESY peak intensities (Wagner et al., 1987) and from results of initial structure calculations (Skelton et al., 1994). Stereospecific assignments for proline $H^\beta$ and valine methyl groups were made as previously described (Zuiderweg et al., 1985; Kline et al., 1989). Criteria based on the observation of slow amide exchange and characteristic NOEs were used in the assignment of hydrogen bond restraints (Wagner et al., 1987); the O···N distance was restrained to 2.5−3.3 Å and the $H^N$···O distance was restrained to 1.7−2.2 Å.

*Calculation of Structures.* Monomer structures were calculated using the DG-II program (Havel, 1991) within the INSIGHT package (Biosym Technology, San Diego, CA). The bounds matrix was subject to triangle smoothing prior to prospective embedding of all atoms in four dimensions. The embedded structures were regularized using the "optimize" option, annealing for 10 000 steps in four-dimensional space while cooling from 200 K with all atom masses set to 1000. Pseudoatoms were introduced where appropriate and the upper bounds to such atoms increased (Wüthrich et al., 1983). The upper bounds of restraints involving methyl groups were increased by 0.5 Å (Tropp, 1980; Koning et al., 1990). Sixty embeds were performed of which 56 structures converged successfully.

Initial dimer structures were obtained by arranging two copies of each monomer structure to have a relative orientation similar to that observed for the monomers within the MIP-1$\beta$ (Lodi et al., 1994) dimer but separated by 15−20 Å. All 56 dimer models were then refined with dynamical simulated annealing (Nilges et al., 1988) using the program X-PLOR (Molecular Simulations, New Haven, CT). Initially, NOE restraints involving protons close to the center of symmetry were enforced as $(1/r^6)^{-1/6}$ sums of the intra- and intermolecular distances since the two possibilities could not be distinguished from the spectra (Nilges, 1993). In subsequent rounds of calculation, most of these restraints were ascribed to a unique interaction as the structures indicated that protons interacting in the alternate fashion were too distant to contribute to the NOE. Experimental restraints were enforced by flat-bottomed square-well potentials with force constants of 50 kcal·mol$^{-1}$·Å$^{-2}$ and 200 kcal·mol$^{-1}$·rad$^{-2}$ for distances and dihedral angles, respectively. Symmetry was enforced by the inclusion of a noncrystallographic symmetry energy term and explicit distance symmetry restraints (Nilges, 1993). Restraints were also included to enforce the peptide bonds to be within 10° of planarity. The structures were annealed at 1000 K for 3750 steps of 1 fs, cooled to 100 K over 10000 steps of 3 fs, and finally subjected to 2000 steps of rEM. The relative weights of force constants during the annealing cycle were varied in a manner identical to that of Fairbrother et al. (1994).

The structures were visually inspected using INSIGHT-II (Biosym Technology, San Diego) or MIDAS (UCSF Computer Graphics Laboratory; Ferrin et al., 1988) running on Silicon Graphics workstations. Inspection of the dimer structures with lowest restraint violation energy indicated that one structure was noticeably out of family in the region of the 30s loop and also had locally higher violations of the restraints in this region. Ignoring this structure, the 20 members of the ensemble with lowest violation energy were subjected to more detailed analysis and have been deposited in the Brookhaven Protein Data Bank (Bernstein et al., 1977). Angular order parameters ($S^{ang}$) were calculated according to the method of Hyberts et al. (1992). A geometric mean structure of RANTES ($\overline{SA}$) was obtained after the ensemble was overlaid onto the structure with lowest restraint violation

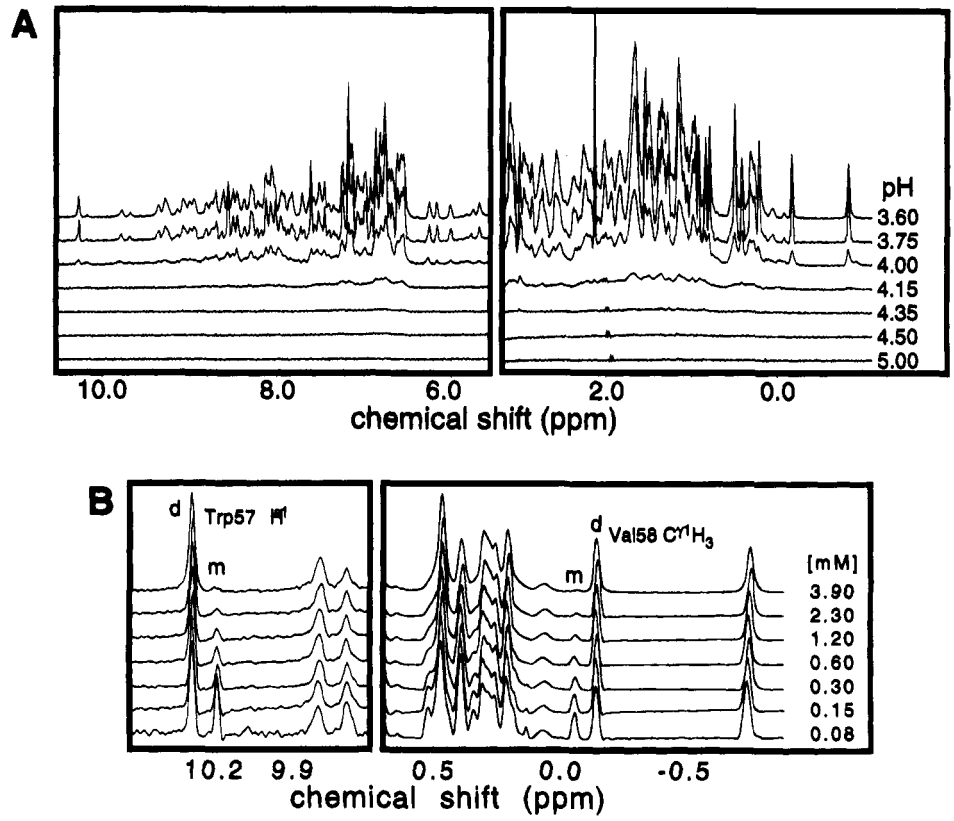


FIGURE 1: 1D $^1$H NMR spectra of RANTES during pH titration (A) and dilution (B) experiments. The pH (A) and total protein concentration (B) are shown at the right of each trace. Spectra were recorded at 500 MHz and 308 K in 25 mM sodium acetate-$d_3$ buffer. In (A) the total protein concentration was 1.3 mM, while in (B) the pH was 3.7. In (B), the labels m and d indicate resonances arising from the monomer and dimer species of the protein.

energy using N, $C^\alpha$, and C atoms of residues 4−66 of both monomers. A regularized mean RANTES structure ($\overline{SA_r}$) was obtained by subjecting the geometric mean to 2000 steps of rEM.

## RESULTS

*Concentration and pH Dependence of the $^1$H NMR Spectrum.* At pH 4.3 and above, RANTES could be concentrated to >1.0 mM in acetate buffer but such solutions were very viscous and *no* protein resonances were observed in 1D NMR spectra. As the pH was lowered from 4.35 to 3.75, the appearance of the 1D spectrum changed abruptly, and a well-resolved spectrum with sharp lines was produced (Figure 1A). This unusual behavior presumably stems from substantial aggregation of the protein at pH 4.35 and above: the aggregate is sufficiently large that the proton resonances are broadened beyond detection. Dynamic light-scattering data collected at pH 4.5 and 0.75 mM protein were best fit by a bimodal distribution of molecules with hydrodynamic radii of 37 and 66 Å. These radii correspond to globular species of approximately 70 and 290 kDa, respectively, confirming that RANTES is indeed heavily aggregated under these conditions.

At pH 3.7 the spectrum contains many upfield-shifted methyl groups and a wide range of amide proton frequencies, indicating that the protein is folded. The peak widths at half-height of the upfield-shifted methyl groups are of the order of 16−18 Hz; this value suggests that RANTES is dimeric under these conditions since similar half-height widths are observed for IL-8 and MGSA (for comparison, values for ubiquitin, an 8 kDa monomeric protein, are <12 Hz). Subsequent analysis revealed spin systems from only 68 residues, indicating that the dimer is symmetric.

During dilution of RANTES from 3.9 to 0.08 mM, changes were observed in the 1D NMR spectrum, with some of the resolved resonances becoming less intense and new resonances appearing and growing in intensity (Figure 1B). Such behavior is characteristic of a dissociation event with slow exchange between the two species. Exchange cross-peaks were readily observed between two upfield-shifted methyl resonances (later determined to be Val58 $C^{\gamma 1}H_3$) in ROESY and NOESY spectra acquired at 0.6 mM concentration. In the dilution series of 1D NMR spectra, the total concentration of protein was known; hence the relative peak sizes of the upfield-shifted methyl group were used to calculate the concentrations of the two forms present. Assuming an equilibrium of the form $nM \rightleftarrows M_n$ (where M represents a protomer and $M_n$ is an aggregate of $n$ protomers), a Hill plot of the data yields a dissociation constant of 35 $\mu$M for a process with $n = 2$ (Figure 2). This analysis does not preclude M from containing multiple copies of a single RANTES monomer, but in light of the line-width data discussed above, this process most likely results from a monomer $\rightleftarrows$ dimer equilibrium.

Lowering the pH below 3.7 caused similar perturbations in the 1D spectrum as dilution, suggesting that dimerization is pH dependent. Between pH 2.5 and pH 2.2 the spectrum remained constant, with resonances from the monomer and dimer present in the ratio of 1 to 7 (total protein concentration of 3 mM). Analysis of the peak intensities of Val58 $C^{\gamma 1}H_3$ during a second dilution series at pH 2.5 yielded a dimer−monomer dissociation constant of 105 $\mu$M. Presumably, the

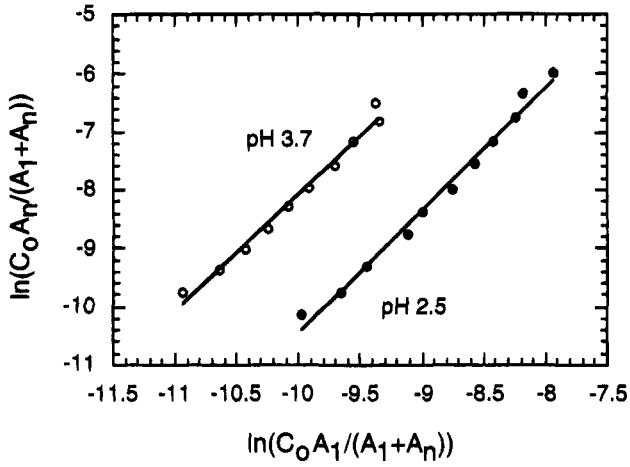


FIGURE 2: Hill plots of monomer:dimer ratios during dilution of RANTES at pH 3.7 (open circles) and 2.5 (filled circles). The quantities plotted are listed on each axis [$C_0$ = total protein concentration (M), $A_1$ = peak area of monomer species and $A_n$ = peak area of aggregated species]. The lines are linear least-squares fits to the data and yield $K_d$ values of 35 $\mu$M and 105 $\mu$M at pH 3.7 and 2.5, respectively.

pH dependence of $K_d$ arises from titration of glutamate and/or aspartate residues near the dimer interface and suggests that the interactions with the charged carboxylate groups of these residues favor dimerization. In order to avoid spectral complications arising from two species undergoing chemical exchange or from aggregation-induced line broadening, data for resonance assignments of RANTES were acquired at pH 3.7 and 4.0 mM total protein concentration. Given the $K_d$ of 35 $\mu$M, approximately 95% of the protein is in the dimeric form under these conditions. Several weak exchange cross-peaks were observed close to the diagonal in ROESY spectra acquired under these concentration. However, *no* other cross-peaks were observed to the exchange partner when this resonance was resolved; hence a semiquantitative analysis of the NOESY and ROESY spectra to generate restraints will not be affected by the small proportion of monomer present. The NMR spectrum remained constant and the protein remained intact (as shown by mass spectrometry) for a period of several weeks at this pH and a temperature of 35 °C.

*Resonance Assignments.* Resonance positions for the 61 amino acids containing a backbone amide proton were identified in COSY, 2Q, and TOCSY spectra acquired from $H_2O$ solution. These were attributed to particular amino acid types on the basis of spin system topology and chemical shift arguments (Wüthrich, 1986). $D_2O$ correlation spectra were analyzed to identify side-chain resonances missing from the $H_2O$ analysis and also to identify the resonance positions of proline residues and the N-terminal serine. The 2Q data were used to confirm cases of chemical shift degeneracy for $H^\beta$ methylene groups, $H^\delta$ groups of proline and arginine, and $H^\epsilon$ groups of lysine. Other instances of resonance degeneracy were assumed on the basis of chemical shift arguments and lack of unassigned cross-peaks in TOCSY and COSY spectra. The 3Q spectrum was used to confirm the positions of the aromatic ring protons of the phenylalanine residues. The amide proton of Ser31 was in fast exchange with the solvent and no correlations to it could be observed in experiments acquired with presaturation. The $H^\alpha$ and $H^\beta$ resonance positions were identified in $D_2O$ solution, and the amide proton chemical shift was inferred from peaks observed in the JR-NOESY spectrum.

After this analysis, four $H^N$–$H^\alpha$ correlations remained unassigned. Peaks in the COSY and TOCSY spectra were very weak, and no NOEs were observed to the backbone amide protons. Since all expected resonances of the protein could be assigned, the assumption was made that these extra peaks arise from the monomeric species present at low abundance. The lack of peaks in the NOESY spectrum indicates that this form of the protein did not complicate a detailed structural analysis of the RANTES dimer.

The identified spin systems were assigned to particular residues in the protein by the observation of sequential $H^N$–$H^N$, $H^\alpha$–$H^N$, and $H^\beta$–$H^N$ NOEs (Wüthrich, 1986). A summary of the NOE data used to make the sequential assignments is shown in Figure 3, and the chemical shifts are listed in the supplementary material.

*Secondary Structure and Dimer Formation.* Analysis of the sequential and medium-range NOE intensities, backbone scalar coupling constants, and some long-range backbone–backbone NOEs indicates that RANTES contains a three-stranded antiparallel $\beta$-sheet (Figure 4A). In addition, there is a C-terminal helix extending from Trp57 to Glu66, with many long-range NOEs indicating that the helix packs on the sheet; this motif is also present in IL-8 (Clore et al., 1990). In IL-8, PF4, and MGSA, the $\beta$-sheet is extended to six strands by the formation of a symmetrical dimer, with the first $\beta$-strand from each monomer aligned in an antiparallel fashion. Such an arrangement leads to the observation of many intermolecular NOEs across the dimer interface (Clore et al., 1989; Fairbrother et al., 1993); *none* of these NOEs are observed in RANTES (Figure 4A, box 1). Thus, although the monomers in IL-8 and RANTES contain the same elements of secondary structure, they do not dimerize in the same fashion.

The present data indicate that there is a further short $\beta$-strand present at the N-terminus of RANTES. NOEs are seen from this strand (Asp6 and Thr7) to the C-terminal strand of the main $\beta$-sheet, including the $H^\alpha$–$H^\alpha$ NOE from Val49 to Asp6 (Figure 4B). These data suggest that the $\beta$-sheet of RANTES is extended to include a short, fourth antiparallel strand (Figure 4A, box 2). This is clearly different from IL-8, where the residues prior to the first cysteine (residues 1–9 in the RANTES numbering used herein) are flexible and disordered in solution (Grasberger et al., 1993). Examination of the structure of IL-8 suggests that the backbone of RANTES would be very contorted in order to accommodate this extra antiparallel strand in the sheet while maintaining the disulfide bond from residue 10 to residue 34. One possible rationalization of the observed NOEs is that dimerization occurs via the N-terminus, with the NOEs shown in Figure 4A (box 2) arising from intermolecular contacts. Such an arrangement explains the presence of these NOEs, the apparent dimeric size of the protein (from line-width data), and the lack of dimer NOEs as found in IL-8. This hypothesis is strengthened by the recent determination of a structure for human MIP-1$\beta$, a C-C chemokine that dimerizes in this fashion (Lodi et al., 1994).

*Solution Structure of RANTES.* Structures have been calculated for the RANTES dimer using distance and dihedral angle restraints generated using NMR data. From inspection of the MIP-1$\beta$ dimer interface (Lodi et al., 1994), many

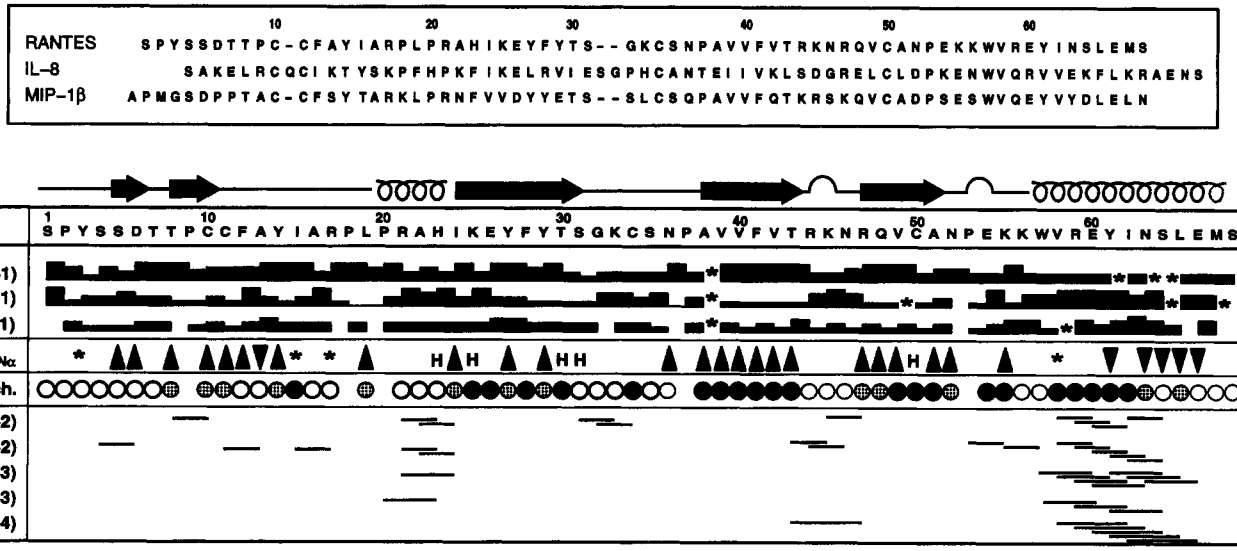


FIGURE 3: Primary sequence and summary of NOEs, coupling constants, and amide proton exchange data for RANTES. The primary sequences of RANTES, IL-8, and MIP-1$\beta$ are aligned according to their common elements of regular secondary structure in the top portion of the figure. In the lower part of the figure the relative intensities of $d_{NN}$, $d_{\alpha N}$, and $d_{\beta N}$ sequential NOEs are indicated by the relative thickness of the bars connecting adjacent residues. $^3J_{HN-H\alpha}$ values greater than 8.0 Hz or less than 6.0 Hz are indicated by the upward or downward pointing arrows, respectively. Asterisks denote that data could not be obtained because of resonance degeneracy; H indicates overlap of the $H^\alpha$ shift with that of $H_2O$. Retarded amide proton exchange with $D_2O$ is indicated by the shaded ($H^N-H^\alpha$ cross-peak observed in the TOCSY experiment started 15 min after the sample was warmed to 35 °C; see Materials and Methods) or filled circles ($H^N-H^\alpha$ cross-peak observed in the TOCSY experiment started 140 min after the sample was warmed to 35 °C). At the bottom of the figure, bars connect residues involved in medium-range NOEs. The sections of helix, $\beta$-strand, and reverse turn present in the structures calculated for RANTES are represented along the top of the figure as coiled lines, filled arrows, and semicircular lines, respectively. Similar elements of secondary structure are observed in IL-8 except for the shaded N-terminal $\beta$-strand.

Table 1: Summary of Input Restraints Used To Calculate the Structure of RANTES

| | | monomer | dimer[a] |
|---|---|---|---|
| $^1H-^1H$ distance restraints[b] | total | 838 | 2078 |
| | intraresidue | 215 | 530 |
| | sequential | 183 | 446 |
| | medium range | 143 | 312 |
| | long range | 297 | 670 |
| | intermolecular | | 118 (2) |
| dihedral angle restraints[c] | $\phi$, $\chi_1$[d] | 45, 22 | 96, 68 |
| stereospecific assignments | $C^\beta H_2$, $CH(C^\gamma H_3)_2$ | 21, 4 | 23, 5 |
| hydrogen bond restraints[e] | $\beta$-sheet | 22 | 44 (4) |
| | α-helix | 10 | 20 |
| total restraints per residue | | 13.8 | 17.0 |

[a] The restraints are counted for both monomers; hence a particular NOE cross-peak will give rise to two restraints. [b] NOE restraints are only counted if they are deemed structurally useful, i.e., if the corresponding upper bound is shorter than that allowed by covalent geometry; all intraresidue NOEs and sequential NOEs to $H^N$ were checked to see if they met this criterion. Values in parentheses indicate $(1/r^6)^{-1/6}$ summed restraints. [c] Additional restraints were also applied to enforce the peptide bond to be within 10° of planarity; however, these are not included in the list of "experimental" restraints. [d] $\chi_1$ dihedral angle restraints with ranges greater than 180° were not enforced in the monomer calculations. [e] Two restraints were included for each hydrogen bond; the number in parentheses indicates intermolecular restraints.

NOEs observed in RANTES were deduced to occur from intermolecular interactions or were sufficiently close to the symmetry axis that they may have contained contributions from both intra- and intermolecular interactions. Initially, structures were calculated for the monomer within the RANTES dimer without these NOEs. Several rounds of calculations were performed, allowing incorporation of restraints ambiguous on the basis of chemical shifts alone, inclusion of stereospecific assignments on the basis of the structures, and correction of typographical errors.

Once optimal monomer structures had been obtained, models were constructed for the dimer on the basis of the MIP-1$\beta$ quaternary structure (see Materials and Methods) and refined by simulated annealing. Intramolecular restraints were duplicated for both monomers, and intermolecular NOEs were explicitly included as intermolecular restraints. NOES with possible intra- and intermolecular contributions were initially incorporated as $(1/r^6)^{-1/6}$ sum restraints (Nilges, 1993). Several rounds of refinement were performed and the structures analyzed to see if any of the ambiguous intermolecular NOEs could be attributed entirely to intra- or intermolecular effects; restraint lists for subsequent calculations were updated accordingly. Due to the better definition of the region close to the center of symmetry in the dimer structure, several additional stereospecific assignments of $\beta$-methylene groups were also made from these structures, and a single intermolecular hydrogen bond was identified from Thr8 $H^N$ to Cys10 O.

The final round of calculations was performed with 1039 NOE-derived distance restraints per monomer; when all experimental restraints are considered, there are 17.0 restraints per residue. Further details of the input to the calculations are provided in Table 1. The 20 structures of lowest residual violation energy at the end of this procedure contained no distance restraint violations greater than 0.11 Å, had excellent energy terms, and form the basis for more detailed analysis. The stereochemical quality of the ensemble was assessed with the program PROCHECK (Laskowski et al., 1993). With regard to the $\phi/\psi$ locations in the Ramachandran diagram, over 98% of residues were in favorable or allowed regions, only one residue consistently was in a generously allowed region, and only one residue of one structure was in a disallowed region. Other parameters by which the quality of the structures may be gauged are listed in Table 2.

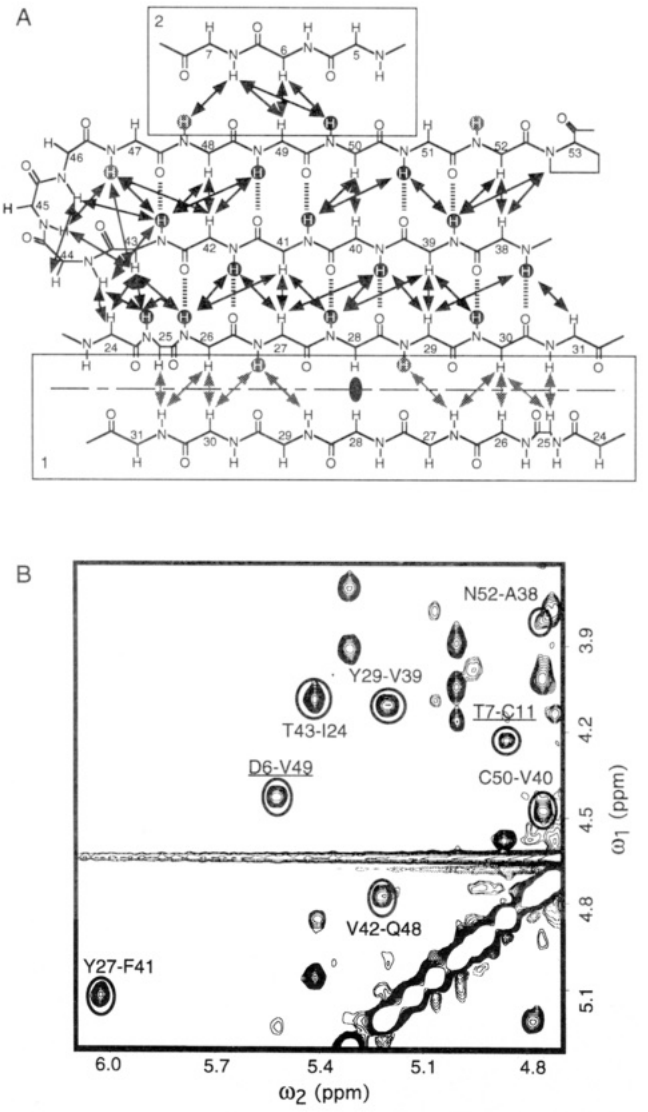


FIGURE 4: (A) Summary of the backbone−backbone NOEs observed in RANTES that define the $\beta$-sheet. NOEs are indicated by arrows, and amide protons undergoing slow exchange with solvent are denoted by shaded or solid circles (see caption to Figure 3). The broken line and solid oval represent the dimer interface and diad axis in IL-8. The NOEs in box 1 are observed in IL-8 but not in RANTES. The NOEs in box 2 are observed in RANTES but not in IL-8. (B) Section of a NOESY spectrum of RANTES acquired from $D_2O$ solution at 308 K with a mixing time of 50 ms. The cross-strand $d_{\alpha\alpha}(i,j)$ NOEs are circled and labeled; the labels for intermolecular NOEs are underlined.

The majority of the RANTES structure is very well defined by the NMR data, with only the three N-terminal residues and the two C-terminal residues showing significant disorder, as judged by local RMSDs and $S^{ang}(\phi,\psi)$ (Figure 5). Ignoring these residues, the mean RMSD of backbone atoms from the mean structure is 0.38 ± 0.06 and 0.53 ± 0.12 Å for the monomer and dimer, respectively. Thus, definition of the dimer interface is slightly worse than the definition of the backbone within each monomer. Other RMSD values are listed in Table 3.

The definitions of Kabsch and Sander (1983) have been used to identify the elements of secondary structure present in each monomer of RANTES. N-Terminal to the C-C motif RANTES contains an isolated $\beta$-bridge at Asp6 ($\beta$b) and a $\beta$-strand ($\beta$N) from Thr8 to Cys10. Both disulfide bonds adopt a left-handed spiral conformation. Beyond the C-C

Table 2: Restraint Violation and Energy Statistics for the Ensemble of RANTES Structures and the Minimized Mean Structure

| | | SA | $\overline{SA_r}$ |
|---|---|---|---|
| energy | total | 328.7 ± 1.7 | 330.2 |
| (kcal•mol$^{-1}$)[a] | bond lengths | 11.7 ± 0.1 | 11.7 |
| | bond angles[b] | 291.4 ± 0.7 | 291.9 |
| | improper | 22.3 ± 0.4 | 22.4 |
| | van der Waals | 2.66 ± 0.55 | 3.26 |
| | NCS | 0.083 ± 0.001 | 0.084 |
| | restraint violation | 0.80 ± 0.45 | 0.86 |
| NOE | no. > 0.01 Å | 21.1 ± 10.4 | 22 |
| violations | no. > 0.1 Å | 0.10 ± 0.45 | 0 |
| | sum (Å) | 0.42 ± 0.21 | 0.42 |
| | maximum (Å) | 0.05 ± 0.03 | 0.04 |
| dihedral angle | no. > 0.1° | 10.5 ± 3.2 | 11 |
| violations | sum (deg) | 1.51 ± 0.71 | 1.87 |
| | maximum (deg) | 0.24 ± 0.11 | 0.42 |
| RMS | intramolecular NOEs (Å) | 0.0045 ± 0.0009 | 0.0025 |
| deviations | intermolecular NOEs (Å) | 0.0017 ± 0.0012 | 0.003 |
| | hydrogen bonds (Å) | 0.0062 ± 0.0022 | 0.009 |
| | dihedral angle restraints (deg) | 0.030 ± 0.014 | 0.035 |
| | ideal bond lengths (Å) | 0.002 ± 0.0 | 0.002 |
| | ideal bond angles (deg) | 0.692 ± 0.001 | 0.692 |
| | ideal improper angles (deg) | 0.352 ± 0.003 | 0.352 |

[a] At the end of the simulated annealing, nonbonded radii were scaled to 0.75 times the value in the parallhdg.pro parameter set, and the force constants for experimental distance restraints, dihedral angle restraints, and noncrystallographic symmetry restraints were 50 kcal•mol$^{-1}$•Å$^{-2}$, 200 kcal•mol$^{-1}$•rad$^{-2}$, and 300 kcal•mol$^{-1}$•Å$^{-2}$, respectively. [b] The bulk of the angle energy results from the incompatibility of proline bond lengths and bond angles in the topallhdg.pro parameter set used in X-PLOR.

motif, the N-loop contains a bend at Ala16/Arg17 followed by a single turn of $3_{10}$ helix (Pro20−His23) before joining the first strand of $\beta$-sheet ($\beta$1). Strand $\beta$1 extends from Ile24 to Thr30, contains a classic $\beta$-bulge at Lys25, and is aligned in an antiparallel fashion with strand $\beta$2 (Ser38 to Arg44). The loop connecting $\beta$1 and $\beta$2 (the 30s loop; Ser31 to Pro37) contains no standard reverse turns but is markedly bent between residues Gly32 and Asn36. A third $\beta$-strand between Arg47 and Ala51 ($\beta$3) packs in an antiparallel fashion on the second edge of strand $\beta$2. The loop connecting $\beta$2 and $\beta$3 (Thr44−Asn46; 40s loop) consists of a distorted 3:5 type I turn (Arg44-Lys45) with a G1 $\beta$-bulge (Asn46) in which the amide proton of Arg47 is hydrogen bonded to $O^{\gamma}$ of Thr43 instead of the backbone carbonyl oxygen; this hydrogen bond is consistent with the observed NOEs, the slow exchange with solvent of Arg47 $H^N$, and the observation of Thr43 $O^{\gamma}H$ in NMR spectra acquired from $H_2O$ solution with presaturation. A final loop (50s loop, Asn52 to Lys55) containing a distorted type I reverse turn (Pro53−Glu54) connects strand $\beta$3 to a regular α-helix extending from Trp57 to Glu66 that packs onto the $\beta$1−$\beta$2−$\beta$3 antiparallel sheet. The secondary structure identified in RANTES is summarized in Figure 6A while the ensemble of structures is depicted in Figure 6B.

In the RANTES dimer, the $\beta$N strands from each monomer are aligned in an antiparallel fashion to create a short $\beta$-sheet with the center of symmetry lying between the two Pro9 residues (Figure 6C). Further intermolecular interactions occur between $\beta$b and strand $\beta$3, as depicted in Figure 4A. Numerous intermolecular side-chain−side-chain contacts are present (Figure 6C): Ser5 $C^{\beta}H_2$ is in contact with Ala13, Ile15, and Val49; Thr7 $C^{\gamma}H_3$ is surrounded by side-chain groups of Pro9, Cys11, Phe28, and Val40; the aromatic ring of Phe12 packs into a cavity created by Thr8, Cys10, and

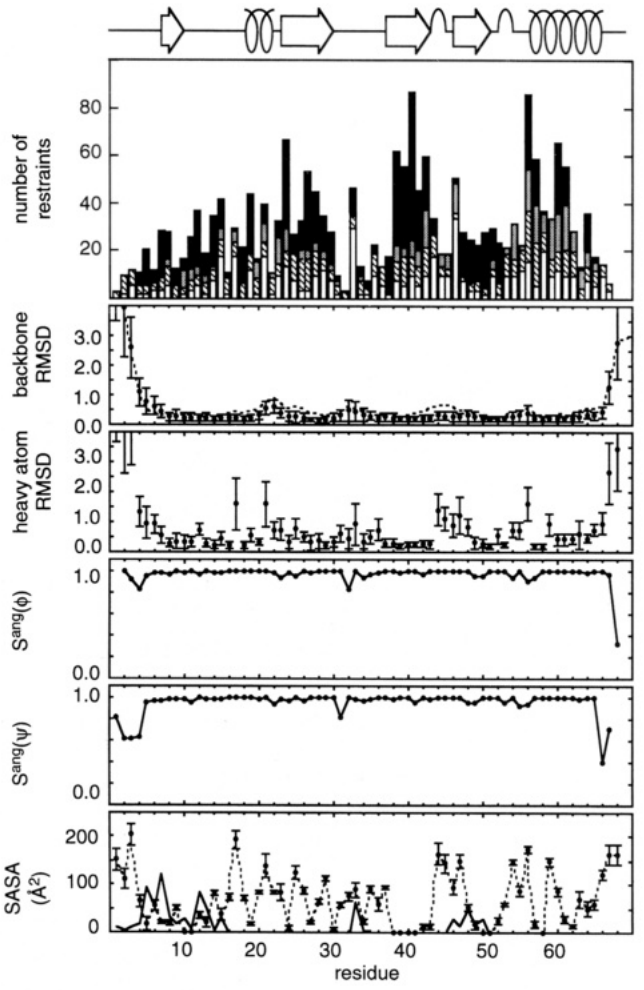


FIGURE 5: Summary of NOE restraints, RMSDs, angular order parameters ($S^{ang}$), and solvent-accessible surface area as a function of residue for the final SA RANTES structures. In the top panel, intraresidue, sequential, medium-range, and long-range (including intermolecular interactions) NOEs are indicated by empty, hatched, shaded, or solid bars, respectively. By-residue RMSDs from the geometric mean structure were calculated after the 20 structures were overlaid to the geometric mean based on N, $C^{\alpha}$, and C atoms of residues 4−66 of a single monomer (data points) or the dimer (dotted line, backbone RMSDs only); error bars indicate standard deviations over the ensemble. $S^{ang}$ for $\phi$ and $\psi$ were calculated according to Hyberts et al. (1992). The contributions of each residue to the solvent-accessible surface area of the dimer were calculated according to the method of Lee and Richards (1971) using a 1.4 Å probe radius. The solid line indicates the additional surface area accessible to solvent in the monomer. The elements of secondary structure present in RANTES are indicated along the top of the figure.

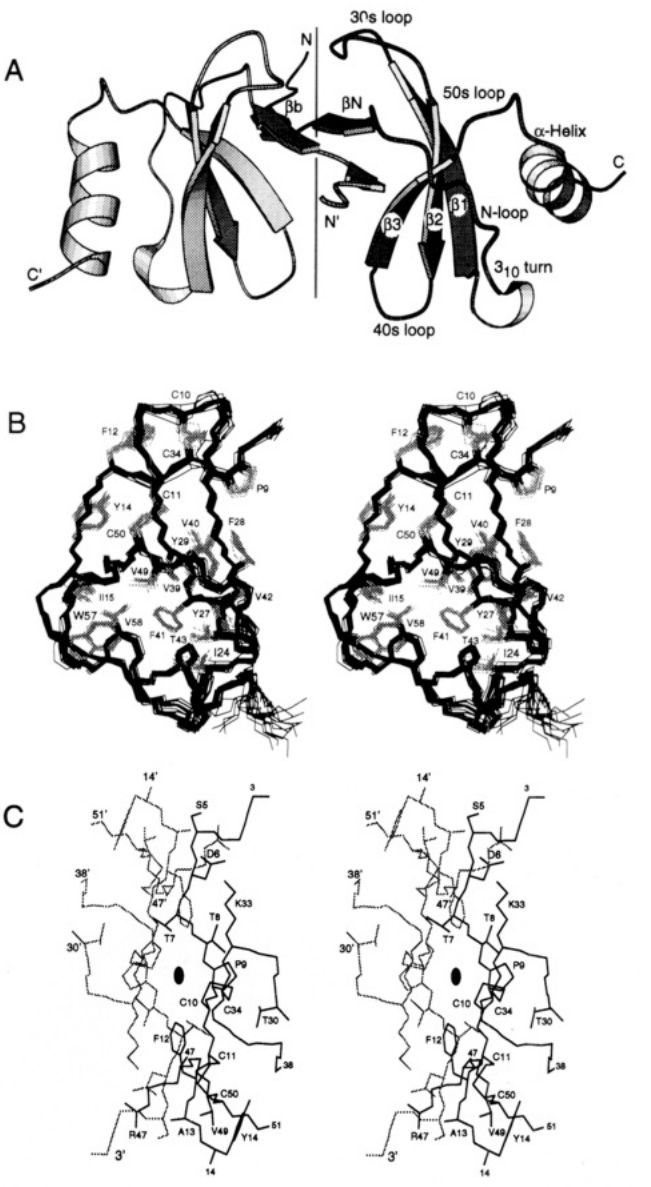


FIGURE 6: (A) Elements of helix (flat coiled ribbons) and sheet (broad arrows) observed in the dimer of RANTES. The vertical line indicates the position of the 2-fold symmetry axis between $\beta$N and $\beta$N′. This view of the minimized mean structure was prepared with the program MOLSCRIPT (Kraulis, 1991). (B) Ensemble of 20 SA RANTES structures. The structures of a single monomer within the dimer are overlaid according to N, $C^{\alpha}$, and N atoms of residues 4−66 of the monomer; residues 1−5 at the N-terminus are not displayed. The heavy atoms of some well-defined side chains are depicted in gray and labeled. (C) Section of the minimized mean structure of the RANTES dimer. The N, $C^{\alpha}$, and C atoms of residues 5−15, 30−38, and 47−51 of both dimers are shown, along with the side-chain heavy atoms of many residues involved in intermolecular contacts. The same atoms are included for both molecules (colored black or gray) but are only labeled in one structure. The black ellipse indicates the position of the diad axis between Pro9 and Pro9′.

Lys33 while the carboxylate group of Asp6 is close to the guanidine group of Arg47 and may be involved in an intermolecular salt bridge. With the exception of the latter interaction, the majority of these contacts do give rise to readily observable intermolecular NOEs. The Asp6−Arg47 salt bridge may be responsible for the pH dependence of dimerization discussed above: at very low pH, the carboxylate group of Asp6 becomes protonated, and the proposed salt bridge no longer makes an energetically favorable contribution to dimerization. The decrease in solvent-accessible surface area in going from the monomer to the dimer is shown in Figure 5 and confirms that residues at the N-terminus (Ser5-Ile15), the 30s loop (Lys33−Cys34), and strand $\beta$3 (Asn46−Cys50) are in intimate contact in the dimer; the total decrease in solvent-accessible surface area on forming the dimer is 780 Å$^2$ per monomer.

## DISCUSSION

*Aggregation of Chemokines and Activity.* Extrapolation of the pH dependence of RANTES dimerization suggests that the dimer is very stable at neutral pH. However, the observed changes in line width indicate that a larger aggregate is predominant at neutral pH, at least at protein

Table 3: Superpositions of RANTES, IL-8, and MIP-1$\beta$ Monomers (Dimers)

| residues[a] | RMSD (Å) of RANTES vs RANTE[b] N, $C^\alpha$, C | RANTES[b] heavy atom | IL-8[c] N, $C^\alpha$, C | MIP-1$\beta$[d] N, $C^\alpha$, C |
|---|---|---|---|---|
| $\beta$-sheet (24−31, 37−43, 47−51) | 0.18 ± 0.04 | 0.51 ± 0.08 | 1.03 ± 0.04 | 0.78 ± 0.03 |
| $\beta$-sheet + $\alpha$-helix (24−31, 37−43, 47−51, 57−66) | 0.24 ± 0.03 | 0.64 ± 0.05 | 1.12 ± 0.05 | 0.74 ± 0.03 |
| $\beta$-sheet + $\alpha$-helix + 40s + 50s loops (24−31, 37−66) | 0.24 ± 0.03 | 0.72 ± 0.05 | 1.18 ± 0.04 | 1.02 ± 0.03 |
| $\beta$-sheet + $\alpha$-helix + 20s + 40s + 50s loops (9−31, 37−66) | 0.28 ± 0.03 | 0.78 ± 0.07 | 1.80 ± 0.04 | 1.39 ± 0.04 |
| $\beta$-sheet + $\alpha$-helix + 20s + 30s + 40s + 50s loops[e] (9−66) | 0.30 ± 0.03 | 0.78 ± 0.07 | 1.97 ± 0.04 | 1.66 ± 0.05 (5.56 ± 0.26) |
| well-defined core[e] (4−66) | 0.38 ± 0.06 (0.53 ± 0.12) | 0.80 ± 0.07 (0.90 ± 0.11) | 3.88 ± 0.11 | 2.43 ± 0.11 (5.52 ± 0.27) |

[a] Residues numbered according to the RANTES sequence. [b] 20 $\overline{SA}$ structures vs $SA_r$. [c] 20 SA RANTES structures vs minimized mean IL-8 structure (PDB accession code 1IL8). [d] 20 SA RANTES structures vs minimized mean MIP-1$\beta$ structure (PDB accession code 1HUM). [e] Values in parentheses indicate comparison of dimer structures.

concentrations greater than 1 mM. The formation of a large, yet soluble, aggregate helps to explain the anomalous behavior of RANTES during *in vitro* competition binding studies reported previously (Neote et al., 1993). Further, the aggregation presumably reduces the number of surface sites on RANTES that are accessible to receptor. This will have an important influence on the specific activity measured during *in vitro* assays if dissociation to smaller species is either kinetically or thermodynamically unfavorable with respect to receptor binding.

Attachment of the chemokine molecules to cell surface glycosaminoglycans is an important aspect in maintaining a chemokine concentration gradient for selective leukocyte trafficking during diapedesis and migration within tissue (Butcher, 1991; Lasky, 1992; Springer, 1994). The association of chemokines with heparin or heparan sulfate has been demonstrated for a number of chemokines (Webb et al., 1993; Witt & Lander, 1994). Presentation of RANTES in this fashion *in vivo* possibly prevents self-aggregation and allows a relatively high surface concentration of chemokine to be generated. However, the formation of aggregates may have a physiological role in limiting the amount of active RANTES circulating in the blood stream, as has been previously suggested for aggregate formation in MIP-1$\alpha$ (Mantel et al., 1993).

The aggregation of RANTES is not unique among the chemokine proteins. The C-X-C protein PF4 crystallizes as a tetramer (Zhang et al., 1994) and has also been shown to participate in a monomer−dimer−tetramer equilibrium in solution (Mayo & Chen, 1989). In the C-C chemokine family, both MIP-1$\alpha$ (Mantel et al., 1993) and MIP-1$\beta$ (Lodi et al., 1994) aggregate extensively near neutral pH, with MIP-1$\beta$ forming a discrete dimer at pH 2.5. These observations raise the question of what aggregation state is present at physiological concentrations and which of these species is responsible for activity. Recently, IL-8 mutants with disrupted dimer interfaces that are monomeric up to millimolar concentrations have been prepared and found to be capable of binding, attracting, and activating neutrophils (Rajarathnam et al., 1994). Similarly, mutational studies with MIP-1$\alpha$ have identified proteins that are monomeric at physiological concentrations and equipotent to wild-type protein in terms of stem cell inhibition and induction of monocyte shape change (Graham et al., 1994). These studies indicate that, for some chemokine functions, the quaternary structure is not important and that useful insight into the structural features required for receptor binding and stimulation may be obtained by comparison of the monomer structures (with the caveat that the determined structure may be influenced by the quaternary interactions). Thus, in the following discussion, comparison of the RANTES structure to the structures previously determined for other chemokines is performed at both the quaternary and tertiary level.

*Comparison of Chemokine Quaternary Structure.* The solution structure of MIP-1$\beta$ has recently been reported (Lodi et al., 1994). This C-C chemokine was found to have secondary and tertiary structure similar to that of IL-8 but a very different quaternary arrangement of the monomers. Dimerization occurred through interaction of the region N-terminal to the C-C motif of one monomer with residues in the 30s loop and strand $\beta$3 of the other monomer, i.e., in a manner similar to that observed for RANTES in the present study. Comparison of the structures of IL-8 and MIP-1$\beta$ (Lodi et al., 1994) or hydrophobic cluster modeling of other chemokines (Covell et al., 1994) has identified key hydrophobic residues either at the N-termini of C-C chemokines or in strand $\beta$1 of C-X-C chemokines that are presumed to dictate the mode of dimerization. The results described herein add credence to the hypothesis that all C-C chemokines dimerize in a fashion similar to that of RANTES or MIP-1$\beta$.

Although residues 9−66 of RANTES and MIP-1$\beta$ are similar at the tertiary level (single monomer backbone atom RMSD of 1.67 Å), the relative arrangement of the two monomers in the dimer is distinctly different (dimer backbone atom RMSD of 5.56 Å; Table 3). The MIP-1$\beta$ dimer is much more extended than that of RANTES (Figure 7) with the separation of Asn46 C$\alpha$ in the two monomers increasing from 9.9 ± 1.0 Å in the RANTES ensemble to 31.5 Å in the minimized mean MIP-1$\beta$ structure. There is very little sequence conservation between RANTES and MIP-1$\beta$ for residues N-terminal to the C-C motif and in the 30s loop (Figure 3). Thus, the modest changes of backbone dihedral angles to accommodate different side chains at the interface may lead to very large displacements of residues far from the interface. For example, Thr7 $C^{\gamma 2}H_3$ in RANTES resides in a pocket formed by Cys11, Cys50, Phe28, and Val40 of the other monomer. Accommodation of the bulkier proline residue (Pro8) in MIP-1$\beta$ requires a reorganization of these intermolecular interactions and produces a more open quaternary structure. Although the difference in quaternary structure may contribute to the particular receptor specificity of MIP-1$\beta$ and RANTES, confirmation of this will require more detailed investigations into the molecular species present under physiological conditions.

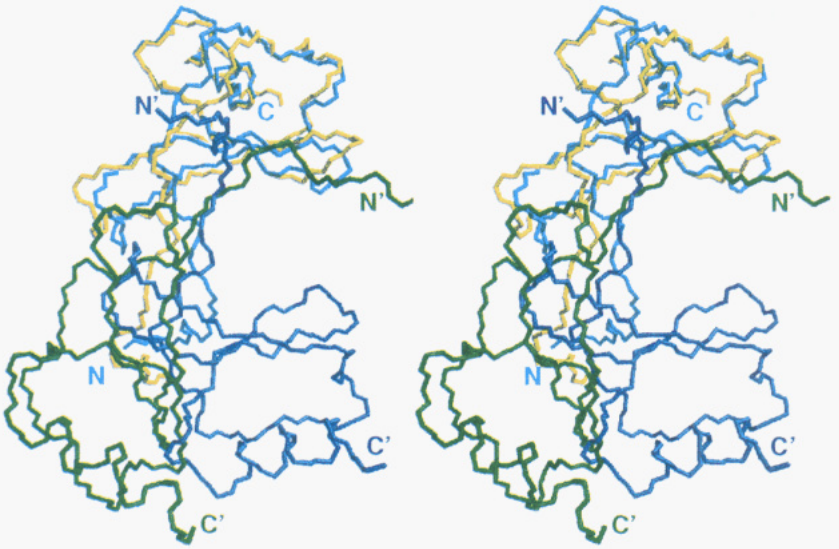


FIGURE 7: Comparison of the quaternary structures of RANTES and MIP-1$\beta$. The minimized mean structures of RANTES (blue and cyan lines) and MIP-1$\beta$ (green and yellow lines; PDB accession code 1HUM) were overlaid using the N, $C^{\alpha}$, and C atoms of residues 9−66 of the top monomer. Different interactions at the dimer interface lead to a substantially different location for the lower monomer.

*Comparison of Chemokine Tertiary Structure.* To date, high-resolution structural studies have been published for IL-8 (Clore et al., 1990; Baldwin et al., 1991), PF4 (St. Charles et al., 1989; Zhang et al., 1994), MIP-1$\beta$ (Lodi et al., 1994), and MGSA (Fairbrother et al., 1994; Kim et al., 1994). IL-8 and MIP-1$\beta$ form the main basis for comparison in this section as a wealth of structure−function studies are available for the former and the latter is the only other published structure of a C-C chemokine. Both NMR and X-ray structures exist for IL-8 (Clore et al., 1990; Baldwin et al., 1991), and differences between them are slight at the monomer level (Clore & Gronenborn, 1991). Thus, comparisons herein are made to the minimized mean NMR structure (PDB accession number 1IL8).

At the secondary structure level, RANTES and IL-8 are very similar, with the triple-stranded $\beta$-sheet (including $\beta$-bulges) and C-terminal α-helix being present in both proteins (Figure 8A), although the helix is six residues longer in IL-8. Backbone heavy atoms for residues in the sheet, helix, and 40s and 50s loops of RANTES may be superposed with an RMSD of 1.18 ± 0.04 Å (Table 3) onto the equivalent atoms of IL-8, in spite of the low sequence identity for these residues (21%). The equivalent folds for the hydrophobic core of the protein result in part from conservative differences between the two sequences. For example, Val39, Val40, and Val49 in RANTES are isoleucine or leucine residues in IL-8. In other cases, a significant increase in the size of one hydrophobic side chain is counterbalanced by a reduction in the size of others. Phe41 is at the center of the hydrophobic core in RANTES, but the equivalent side chain in IL-8 is a valine. The much bulkier side chain in RANTES is partially accommodated by a compensatory decrease in the size of the side chain at position 51 (alanine in RANTES, leucine in IL-8; Figure 8B). Variations in the exact nature of the hydrophobic packing lead to differences in the backbone of the secondary structure elements: for example, the decrease in size of the residue at position 65 (leucine in RANTES and phenylalanine in IL-8) causes strand $\beta$1 to shift ~2 Å toward the helix.

Figure 9 shows the displacement of backbone atoms between RANTES and IL-8 after superposition of residues 24−31 and 37−66. Significant differences are observed for the residues N-terminal to the C-C motif, two residues of the N-loop and the $3_{10}$ helical turn (residues 18−23), and the 30s loop, with some backbone atoms shifting by as much as 4 Å (see also Figure 8A). The shift in the N-loop residues results from the different hydrophobic packing between this peptide segment and the sheet and helix: Val41 in strand $\beta$2 of IL-8 is replaced by the bulkier Phe41 in RANTES (Figure 8B); Phe19 in the N-loop of IL-8 is replaced by the smaller Leu19 in RANTES (Figure 8B); and Val61 in the helix of IL-8 is replaced by the larger Tyr61 of RANTES (Figure 8C). The net result of these changes is to put a pronounced kink at residue 19 in the N-loop of RANTES and to shift the residues in the $3_{10}$ helical turn (Figure 8).

The positions of the second and fourth cysteine, relative to the elements of regular secondary structure, are very similar in RANTES and IL-8 due to the disulfide bond between them and the location of the latter in strand $\beta$3. However, in RANTES the removal of two residues in the 30s loop (to which the first cysteine is disulfide linked) and the lack of a residue between the first and second cysteine cause a distinct change in the relative positions of the first and third cysteine residues in the two structures. The extra residues in IL-8 allow the 30s loop and the N-terminus to be in closer proximity (Arg6 $C^{\alpha}$−His33 $C^{\alpha}$ = 5.3 Å) relative to the case in RANTES (Pro9 $C^{\alpha}$−Lys33 $C^{\alpha}$ = 8.8 ± 0.2 Å). In addition, the buried loop residue Glu38 of IL-8 is replaced by alanine in RANTES, with the backbone atoms of residues at the tip of the 30s loop occupying some of the space vacated by the bulkier glutamate side chain. The net result of these amino acid changes is to fold the tip of the loop (Cys34) back toward the rest of the protein in RANTES (i.e., the 30s loop does not extend as far from the bulk of the protein) and change the direction of the main-chain atoms prior to the first cysteine by about 90° (Figure 10).

Backbone heavy atoms of RANTES residues 24−31 and 37−66 may be overlaid on the equivalent residues of MIP-1$\beta$ (Lodi et al., 1994) with an RMSD of 1.02 ± 0.04 Å, indicating that the secondary structures of these two proteins are also similar. The backbone atom deviations following such an overlay (Figure 9) identify significant differences

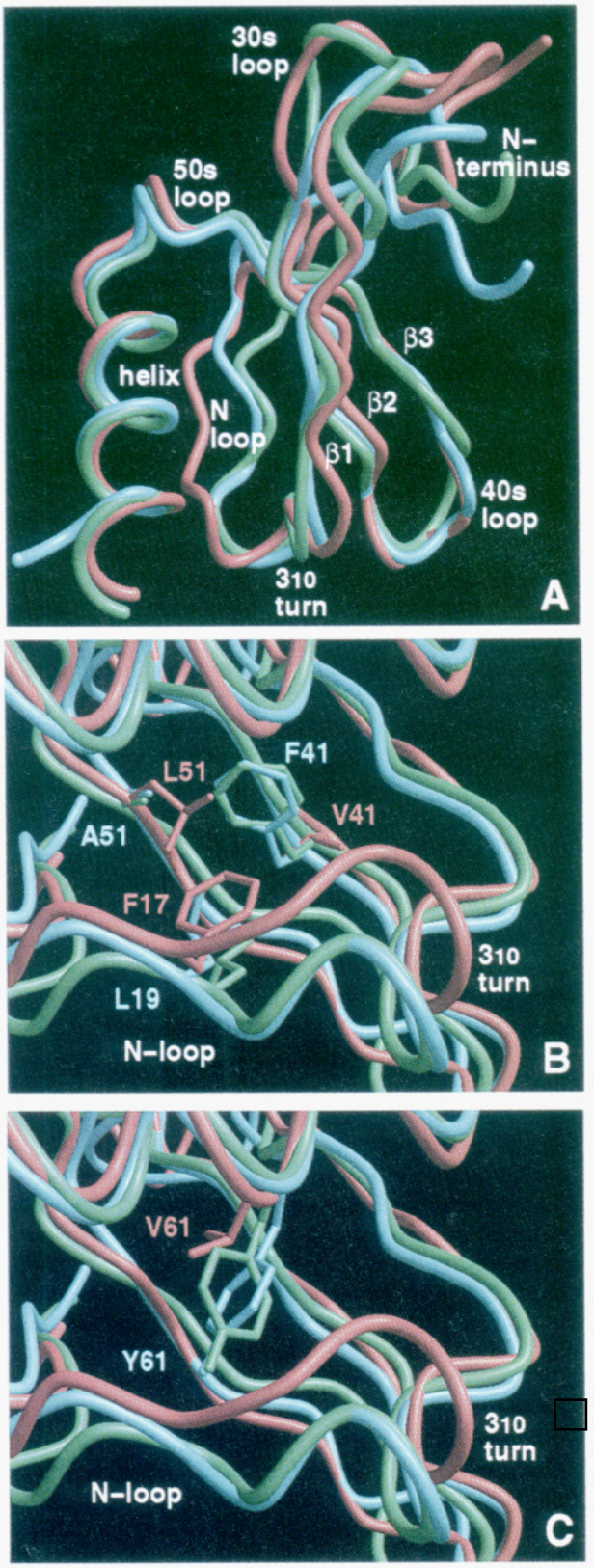


FIGURE 8: Comparison of the monomer structures of RANTES (blue), IL-8 (pink), and MIP-1$\beta$ (green). (A) Global view of the backbone fold (residues 6−68 of RANTES). (B) Close-up of the side chains responsible for the differential packing of the N-loop onto the $\beta$-sheet. (C) Close-up of the side chains responsible for the relative movement of the C-terminal helix and the $3_{10}$ helical turn. In all panels, the overlay is based on the N, $C^{\alpha}$, and C atoms of residues 24−31 and 37−66, and the backbone and side-chain positions are represented by the thick and thin tubes, respectively. In (B) and (C), the view is looking down onto the $\beta$-sheet; the three strands are at the rear of the figure while the edge of the helix and the N-loop are in the foreground at the top and bottom, respectively, of each panel. For RANTES, the geometric mean coordinates were used in (A), and the minimized mean coordinates were used in (B) and (C). Coordinates for IL-8 and MIP-1$\beta$ were obtained from the Brookhaven Data Bank, accession numbers 1IL8 and 1HUM, respectively.

between these structures for the residues prior to the first cysteine, residues 15−18 in the N-loop, the 30s loop and the 40s loop. The differences at the N-terminus and in the 30s loop are primarily the result of the alternate dimer geometry in the two proteins. The changes in the 40s loop are associated with a change in the turn type from the distorted 3:5 type I turn in RANTES (see above) to a series of bends in MIP-1$\beta$. Finally, the changes in the N-loop result from movement of strand $\beta$3, onto which residues 15−18 pack, and also from the orientation of the side chain of residue 55. In RANTES, this residue is a solvent-exposed lysine whereas in MIP-1$\beta$ it is a partially buried glutamate residue that inserts itself between the 50s and N-loop forming a hydrogen bond to the indole proton of residue Trp57, thereby creating a bulge in the N-loop.

*Biological Consequences of the RANTES Structure.* Two receptors that specifically bind to C-X-C but not C-C chemokines have been cloned and characterized (Lee et al., 1992). More recently, two receptors with different specificity for C-C chemokines have been cloned and characterized (Neote et al., 1993b; Charo et al., 1994). In addition, a "promiscuous" receptor has also been identified on red blood cells that is capable of binding both C-X-C and some C-C proteins (Neote et al., 1993a). Comparison of the structures of C-C and C-X-C chemokines allows hypotheses to be made about which elements of the structures are responsible for the different receptor binding and functional properties of the subfamilies.

Amino acid substitutions may lead to differences in specificity of ligand−receptor interactions either by changing the physicochemical properties of side chains on the ligand surface that interact directly with the receptor or by altering residues in the core of the ligand leading to a change in surface shape. As an example of the former kind of analysis, the "ELR" motif preceding to the first cysteine is known to be important for activity in IL-8 (Hébert et al., 1991), yet is not present in the C-C chemokines. Thus, the C-C chemokine receptors must have different side-chain specificity than the C-X-C chemokine receptors for this region, if they interact with these residues at all. Generally, such interactions are hard to predict from the limited sequences available from naturally occurring chemokines (even with the aid of three-dimensional structures), and we defer this type of analysis until there is a more complete database of point mutants and their effect on C-C chemokine function. The structural differences between IL-8, MIP-1$\beta$, and RANTES described above fall into the latter category, and these do provide some insight into those regions of the protein surface that are important for receptor interaction. The differences in conformation of the N-loop and the 30s loop may in part be responsible for the inability of RANTES to bind to either of the IL-8 receptors and *vice versa*. Indeed, preparation of IL-8 chimeric proteins based on the sequence of IP10 indicates that fully active analogs with activity equivalent to IL-8 are only obtained after residues 4−22, 30−35, and Leu49 of IL-8 are substituted into the IP10 framework (Clark-Lewis et al., 1994). Further, structural differences

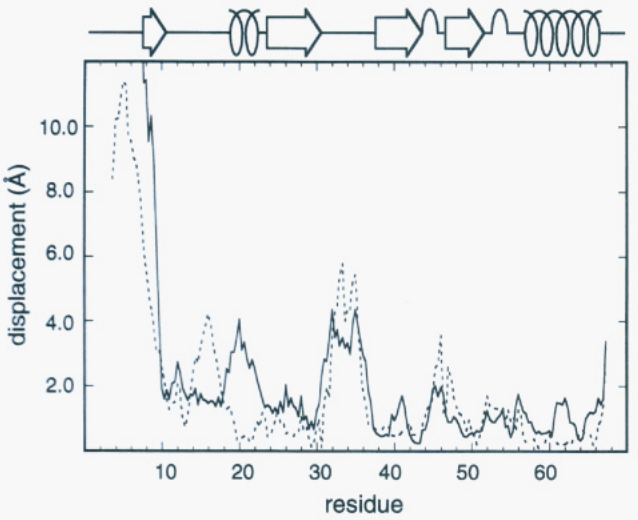


FIGURE 9: Displacement of backbone atoms of IL-8 (solid line) and human MIP-1$\beta$ (dotted line) relative to the RANTES geometric mean NMR structure after alignment using N, $C^{\alpha}$, and C atoms of residues 24−31 and 37−66 (RANTES numbering; see Figure 3 for equivalent IL-8 residues). The minimized mean structures of IL-8 and MIP-1$\beta$ were used for this analysis (PDB accession numbers 1IL8 and 1HUN, respectively). The elements of secondary structure within RANTES are indicated along the top of the figure.

between MGSA and IL-8 in the N-loop and 30s loop have been postulated to give rise to the differential binding of MGSA to the IL-8 receptors (Fairbrother et al., 1994).

With regard to the 30s loop conformation, RANTES, MIP-1α, MIP-1$\beta$, and I309 have two fewer residues and the MCP proteins have one fewer residue in the loop compared to members of the C-X-C subfamily. In addition, we note that all C-X-C proteins contain a glutamate or glutamine at position 38 in the RANTES numbering scheme that is not exposed to solvent. In MGSA the equivalent glutamate is not well-defined by the NMR-derived restraints due to chemical shift degeneracy (Fairbrother et al., 1994), but in PF4 (St. Charles et al., 1989) and both IL-8 structures (Clore et al., 1990; Baldwin et al., 1991), hydrogen bonds are observed from this side chain to backbone amide protons in the C-X-C motif, suggesting that this interaction may be important in positioning the N-terminus with respect to the 30s loop. However, in all C-C chemokines, the equivalent residue is much smaller than a glutamate (glycine, serine, or alanine) and in only one case (Ser40 of MIP-1α) can the side chain accept a hydrogen bond. Thus, it seems likely that, in all C-C proteins, the conformation of this loop is dramatically different from the C-X-C proteins, as described above in the comparison of RANTES and IL-8.

Inspection of primary sequences of chemokines indicates that residue 41 is always phenylalanine and residue 51 is always alanine in the C-C proteins, while these residues are alanine (or valine in the case of IL-8) and leucine, respectively, for the C-X-C proteins. As discussed above, these hydrophobic changes and the presence of a bulky hydrophobic residue at position 61 in the helix are responsible for a pronounced difference in the backbone orientation of residues 19−23 of the N-loop (including the $3_{10}$ helical turn) between RANTES and IL-8. Given the similarities in conformation of these residues but the pronounced differences in residues 15−18 of the N-loop (see above) when MIP-1$\beta$ and RANTES are compared (Figures 8 and 10), the conformation of the N-loop as a whole may be responsible

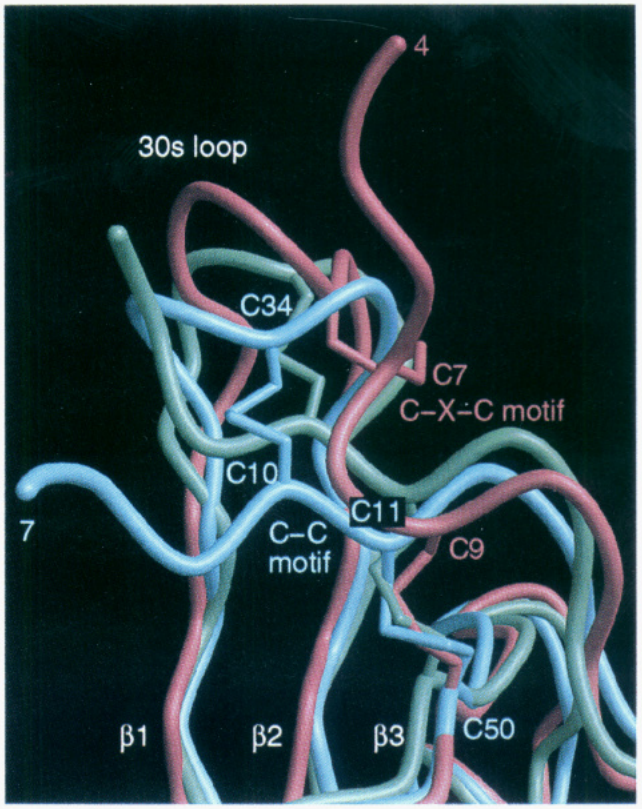


FIGURE 10: Comparison of the orientation of the N-terminus and 30s loop of RANTES, IL-8, and MIP-1$\beta$. The side chains of the cysteine residues are represented in ball-and-stick fashion. Residues 1−5 of RANTES and MIP-1$\beta$ and residues 1−3 of IL-8 have been omitted from this figure. Other details are the same as in Figure 8.

for the low affinity of C-X-C chemokines and the differential affinity of C-C chemokines for the C-C chemokine receptors.

The different quaternary structures of IL-8 and MIP-1$\beta$ have been attributed to hydrophobic residues at the N-terminus of C-C chemokines or in strand $\beta$1 of C-X-C chemokines (Covell et al., 1994). The activity of designed monomeric forms of IL-8 and MIP-1α (Graham et al., 1994; Rajarathnam et al., 1994) and analytical ultra centrifugation studies of IL-8, MCP-1, and I-309 (Burrows et al., 1994; Paolini et al., 1994) suggest that the monomeric form of all chemokines may be functionally important at the low physiological concentrations expected in a biological milieu. The hydrophobic residues responsible for aggregation at high concentration will be solvent accessible in the monomeric state, raising the possibility that they may be important for receptor recognition and activation. The different quaternary structures observed for the IL-8, MIP-1$\beta$, and RANTES at high concentration may be a fortuitous result of the different hydrophobic surfaces required to perform their respective functions.

Mutational studies involving residues at the dimer interface of RANTES may help to shed light on the importance of the quaternary structure to the activity of this protein. More generally, the present structural studies have identified several regions of RANTES where the structure is different from that of other C-C and C-X-C chemokines. These residues may be important for functional differentiation between and within the two chemokine subfamilies. As such, these results provide a guide for mutational studies, targeting residues that will likely have an effect on function when they are mutated. Such studies are currently being designed and will help to

increase our understanding of the complex interplay between these cytokines and their receptors.

## ACKNOWLEDGMENT

We thank Dr. Wayne Fairbrother for many useful discussions and for providing the MGSA coordinates prior to release by Brookhaven and Dr. Jim Bourell for performing mass spectrometric analyses of RANTES.

## SUPPLEMENTARY MATERIAL AVAILABLE

A table containing the chemical shift assignments of RANTES and a section of the $H_2O$ TOCSY spectrum ($\tau_m$ = 75 ms) of RANTES (4 pages). Ordering information is given on any current masthead page.

## REFERENCES

Akke, M., Skelton, N. J., Kördel, J., & Chazin, W. J. (1991) in *Techniques in Protein Chemistry II* (Villafranca, J. J., Eds.) pp 401−408, Academic Press, Inc., Boca Raton, FL.

Aue, W. P., Bartholdi, E., & Ernst, R. R. (1975) *J. Chem. Phys. 64*, 2229−2246.

Baggiolini, M., Dewald, B., & Moser, B. (1994) *Adv. Immunol. 55*, 97−171.

Baldwin, E. T., Weber, I. T., St. Charles, R., Xuan, J. C., Appella, E., Yamada, M., Matsushima, K., Edwards, B. F. P., Clore, G. M., Gronenborn, A. M., & Wlowdower, A. (1991) *Proc. Natl. Acad. Sci. U.S.A. 88*, 502−506.

Bax, A., & Freeman, R. (1981) *J. Magn. Reson. 44*, 542−561.

Bax, A., & Davis, D. G. (1985) *J. Magn. Reson. 65*, 355−360.

Beck, L. A., Schall, T. J., Beall, L. D., Leopold, D., Bickel, C., Baroody, F., Naclerio, R. M., & Schleimer, R. P. (1994) *J. Allergy Clin. Immunol. 93*, 234.

Bernstein, F. C., Koetzle, T. F., Williams, G. J. B., Meyer, E. F., Jr., Brice, M. D., Rodgers, J. R., Kennard, O., Shimanouchi, T., & Tasumi, M. (1977) *J. Mol. Biol. 112*, 535−542.

Bodenhausen, G., Kogler, H., & Ernst, R. R. (1984) *J. Magn. Reson. 58*, 370−388.

Bothner-By, A. A., Stephens, R. L., Lee, J.-m., Warren, C. D., & Jeanloz, R. W. (1984) *J. Am. Chem. Soc. 106*, 811−813.

Braunschweiler, L., & Ernst, R. R. (1983) *J. Magn. Reson. 53*, 521−528.

Braunschweiler, L., Bodenhausen, G., & Ernst, R. R. (1983) *Mol. Phys. 48*, 535−560.

Burrows, S. D., Doyle, M. L., Murphy, K. P., Franklin, S. G., White, J. R., Brooks, I., Nulty, D. E., Scott, M. O., Knutson, J. R., Porter, D., Young, P. R., & Hensley, P. (1994) *Biochemistry 33*, 12741−12745.

Butcher, E. C. (1991) *Cell 67*, 1033−1036.

Cavanagh, J., & Rance, M. (1992) *J. Magn. Reson. 96*, 670−678.

Charo, I. F., Myers, S. J., Herman, A., Franci, C., Connolly, A. J., & Coughlin, S. R. (1994) *Proc. Natl. Acad. Sci. U.S.A. 91*, 2752−2756.

Clark-Lewis, I., Dewald, B., Loechester, M., Moser, B., & Baggiolini, M. (1994) *J. Biol. Chem. 269*, 16075−16081.

Clore, G. M., & Gronenborn, A. M. (1991) *J. Mol. Biol. 217*, 611−620.

Clore, G. M., Appella, E. A., Yamada, M., Mataushima, K., & Gronenborn, A. M. (1989) *J. Biol. Chem. 264*, 18907−18911.

Clore, G. M., Appella, E., Yamada, M., Matsushima, K., & Gronenborn, A. M. (1990) *Biochemistry 29*, 1689−1696.

Clore, G. M., Bax, A., & Gronenborn, A. M. (1991) *J. Biomol. NMR 1*, 13−22.

Clubb, R. T., Fergusen, S. B., Walsh, C. T., & Wagner, G. (1994) *Biochemistry 33*, 2761−2772.

Covell, D. G., Smythers, G. W., Gronenborn, A. M., & Clore, G. M. (1994) *Protein Sci. 3*, 2064−2072.

Fairbrother, W. J., Reilly, D., Colby, T., & Horuk, R. (1993) *FEBS Lett. 330*, 302−306.

Fairbrother, W. J., Reilly, D., Colby, T. J., Hesselgesser, J., & Horuk, R. (1994) *J. Mol. Biol. 242*, 252−270.

Ferrin, T. E., Huang, C. C., Jarvis, L. E., & Langridge, R. (1988) *J. Mol. Graphics 6*, 13−27.

Graham, G. J., MacKenzie, J., Lowe, S., Tsang, M. L.-S., Weatherbee, J. A., Issacson, A., Medicherla, J., Fang, F., Wilkinson, P. C., & Pragnell, I. B. (1994) *J. Biol. Chem. 269*, 4974−4978.

Grasberger, B. L., Gronenborn, A. M., & Clore, G. M. (1993) *J. Mol. Biol. 230*, 364−372.

Gronenborn, A. M., & Clore, G. M. (1991) *Protein Eng. 4*, 263−269.

Havel, T. F. (1991) *Prog. Biophys. Mol. Biol. 56*, 43−78.

Hébert, C. A., Vitangcol, R. V., & Baker, J. B. (1991) *J. Biol. Chem. 266*, 18989−18994.

Hébert, C. A., Chuntharapai, A., Smith, M., Colby, T., Kim, J., & Horuk, R. (1993) *J. Biol. Chem. 268*, 18459−18553.

Hyberts, S., Goldberg, M. S., Havel, T. F., & Wagner, G. (1992) *Protein Sci. 1*, 736−751.

Kabsch, W., & Sander, C. (1983) *Biopolymers 22*, 2577−2637.

Kameyoushi, Y., Dörschner, A., Mallet, A. I., Christophers, E., & Schröder, J. M. (1992) *J. Exp. Med.*, 587−592.

Kelner, G. S., Kennedy, J., Bacon, K. B., Kleyensteuber, S., Largeaspada, D. A., Jenkins, N. A., Copeland, N. G., Bazan, J. F., Moore, K. W., Schall, T. J., & Zlotnik, A. (1994) *Science 266*, 1395−1399.

Kim, K.-S., Clark-Lewis, I., & Sykes, B. D. (1994) *J. Biol. Chem. 269*, 32909−32915.

Kline, A. D., Braun, W., & Wüthrich, K. (1989) *J. Mol. Biol. 104*, 675−724.

Koning, T. M. G., Boelens, R., & Kaptein, R. (1990) *J. Magn. Reson. 90*, 111−123.

Kraulis, P. (1991) *J. Appl. Crystallogr. 24*, 946−950.

Kumar, A., Ernst, R. R., & Wüthrich, K. (1980) *Biochem. Biophys. Res. Commun. 95*, 1−6.

Kuna, P., Reddigari, S. R., Schall, T. J., Rucinski, D., Viksman, M. Y., & Kaplan, A. P. (1992) *J. Immunol. 149*, 636−642.

Laskowski, R. A., MacArthur, M. W., Moss, D. S., & Thornton, J. M. (1993) *J. Appl. Crystallogr. 26*, 283−291.

Lasky, L. A. (1992) *Science 258*, 964−969.

Lee, B., & Richards, F. M. (1971) *J. Mol. Biol. 55*, 379−400.

Lee, J., Horuk, R., Rice, G. C., Bennett, G. L., Camerato, T., & Wood, W. I. (1992) *J. Biol. Chem. 267*, 16283−16287.

Lindley, I. J. D., Westwick, J., & Kunkel, S. L. (1993) *Immunol. Today 14*, 24.

Lodi, P. J., Garrett, D. S., Kuszewski, J., Tsang, M. L.-S., Weatherbee, J. A., Leonard, W. J., Gronenborn, A. M., & Clore, G. M. (1994) *Science 263*, 1762−1767.

Mantel, C., Kim, Y. J., Cooper, S., Kwon, B., & Broxmeyer, H. E. (1993) *Proc. Natl. Acad. Sci. U.S.A. 90*, 2232−2236.

Marion, D., & Wüthrich, K. (1983) *Biochem. Biophys. Res. Commun. 113*, 967−974.

Mayo, K. H., & Chen, M.-J. (1989) *Biochemistry 28*, 9469−9478.

Miller, M. D., & Krangel, M. S. (1992) *CRC Crit. Rev. Immunol. 12*, 17−46.

Moser, B., Dewald, B., Barella, L., Schumacher, C., Baggiolini, M., & Clark-Lewis, I. (1993) *J. Biol. Chem. 268*, 7125−7128.

Neote, K., Darbonne, W., Ogez, J., Horuk, R., & Schall, T. J. (1993a) *J. Biol. Chem. 268*, 12247−12249.

Neote, K., DiGregorio, D., Mak, J. Y., Horuk, R., & Schall, T. J. (1993b) *Cell 72*, 415−425.

Nilges, M. (1993) *Proteins 17*, 297−309.

Nilges, M., Clore, G. M., & Gronenborn, A. M. (1988) *FEBS Lett. 239*, 317−324.

Oppenheim, J. J., Zachariae, C. O. C., Mukaida, N., & Matsushima, K. (1991) *Annu. Rev. Immunol. 9*, 617−48.

Otting, G., Widmer, H., Wagner, G., & Wüthrich, K. (1986) *J. Magn. Reson. 66*, 187−193.

Paolini, J. F., Willard, D., Consler, T., Luther, M., & Krangel, M. S. (1994) *J. Immunol. 153*, 2704−2716.

Plateau, P., & Guéron, M. (1982) *J. Am. Chem. Soc. 104*, 7310−7311.

Rajarathnam, K., Sykes, B. D., Kay, C. M., Dewald, B., Geiser, T., Baggiolini, M., & Clark-Lewis, I. (1994) *Science 264*, 90−92.

Rance, M., & Wright, P. E. (1986) *J. Magn. Reson. 66*, 372−378.

Rance, M., Sørensen, O. W., Bodenhausen, G., Wagner, G., Ernst, R. R., & Wüthrich, K. (1983) *Biochem. Biophys. Res. Commun. 117*, 479−485.
Rot, A., Krieger, M., Brunner, T., Bischoff, S. C., Schall, T. J., & Dahinden, C. A. (1992) *J. Exp. Med. 176*, 1489−1495.
Schall, T. J. (1991) *Cytokine 3*, 165−183.
Schall, T. J. (1994) in *The cytokines* (Thomson, A., Ed.) pp 419−460, Academic Press, New York.
Schall, T. J., Jongstra, J., Dyer, B. J., Jorgensen, J., Clayberger, C., Davis, M. M., & Krensky, A. M. (1988) *J. Immunol. 141*, 1018−1025.
Schall, T. J., Bacon, K., Toy, K. J., & Goeddel, D. V. (1990) *J. Immunol. 147*, 2215−2221.
Skelton, N. J., Garcia, K. C., Goeddel, D. V., Quan, C., & Burnier, J. P. (1994) *Biochemistry 33*, 13581−13592.
Springer, T. A. (1994) *Cell 76*, 301−314.
St. Charles, R., Waltz, D. A., & Edwards, B. F. P. (1989) *J. Biol. Chem. 264*, 2092−2099.
Tropp, J. (1980) *J. Chem. Phys. 72*, 6035−6043.
Wagner, G., Braun, W., Havel, T. F., Schaumann, T., Go, N., & Wüthrich, K. (1987) *J. Mol. Biol. 196*, 611−639.
Webb, L. M. C., Ehrengruber, M. U., Clark-Lewis, I., Baggiolini, M., & Rot, A. (1993) *Proc. Natl. Acad. Sci. U.S.A. 90*, 7158−7162.
Witt, D. P., & Lander, A. D. (1994) *Curr. Biol. 4*, 394−400.
Wüthrich, K. (1986) *NMR of Proteins and Nucleic Acids*, Wiley, New York.
Wüthrich, K., Billeter, M., & Braun, W. (1983) *J. Mol. Biol. 169*, 949−961.
Yip, P. (1990) *J. Magn. Reson. 90*, 382−383.
Zhang, X., Chen, L., Bancroft, D. P., Lai, C. K., & Maione, T. E. (1994) *Biochemistry 33*, 8361−8366.
Zuiderweg, E. R. P., Boelens, R., & Kaptein, R. (1985) *Biopolymers 24*, 601−610.

BI942537T